Supporting Information for "Vertical Land Motion from Present-Day Deglaciation in the Wider Arctic"

Carsten Ankjær Ludwigsen[1], Shfaqat Abbas Khan[1], Ole Baltazar Andersen[1]and Ben Marzeion[2]

[1]DTU Space, Technical University of Denmark
[2]Institute of Geography and MARUM Center for Marine Environmental Sciences, University of Bremen, Germany

Contents of this file

S1 Description of glacier ice model

As initial conditions, we use glacier outlines obtained from RGI6.0 (Pfeffer et al., 2014). The time stamp of these outlines differs between glaciers, but is typically around the year 2000. To obtain results before this time, the model uses an iterative process to find the glacier geometry in the year of initialization (e.g., 1901) that results in the observed glacier geometry in the year of the outlines time stamp (e.g., 2000) after the model was run forward.

The model relies on monthly temperature and precipitation anomalies to calculate the specific mass balance of each glacier. Here, we use the mean of seven different reanalysis products as boundary conditions. Temperature is used to estimate the ablation of glaciers following a temperature-index melt model, and to estimate the solid fraction of total precipitation, which is used to estimate accumulation.

Mass balance data for each glacier is distributed over the glacier according to a mathematical approximation, assuming conservation of mass and that the glacier has a elevation gain at the top which becomes a elevation decline further down the glacier. The altitude where the elevation change goes from positive to negative, E, is approximated by a simple function of the glacial altitude (Z) and the averaged ice height change, ($\bar{\mathrm{h}} = \rho b A^{-1}$), and ρ is the ice density (917 kg m^{-3}). Note that E is different from the equilibrium line altitude (ELA).

$$\mathrm{E} = (1 - \bar{\mathrm{h}})\tilde{Z} \tag{S1}$$

where $\tilde{Z}$ is the median glacial height. For every glacier we define a distribution function, $D(i)$, where i represents a grid cell of the glacier:

$$D(i) = \quad 1 - \exp\left(\frac{\left(2-\bar{\mathrm{h}}\right)(\mathrm{E}-Z(i))}{Z_{max}}\right) \tag{S2}$$

For all glaciers, is the elevation change assumed to be exponentially declining with height, $Z(i)$. The fraction in the exponential term makes sure that glaciers that on average gains

Corresponding author: Carsten Ankjær Ludwigsen, caanlu@space.dtu.dk

up to 2 m height, will have an elevation loss in the bottom of the glacier and elevation gain at the top, unless E is equal or to Z_{max}, in which case, the whole glacier will be loosing height.

The elevation change, dh/dt, is found by normalizing D, multiplying with the total mass balance, b, and converted to a height change by dividing with $\rho = 917$ kg m^{-3}.

$$\frac{dh(i)}{dt} = \frac{b}{\rho}\hat{D}(i) \qquad \text{where,} \tag{S3}$$

$$\hat{D}(i) = \frac{D(i)}{\sum_{i=1}^{k} D(i)} \tag{S4}$$

S1.1 Data availability

The ice model is available as a NetCDF-4 file on `data.dtu.dk/articles/Arctic_Vertical_Land_Motion_5x5_km_/12554489`.

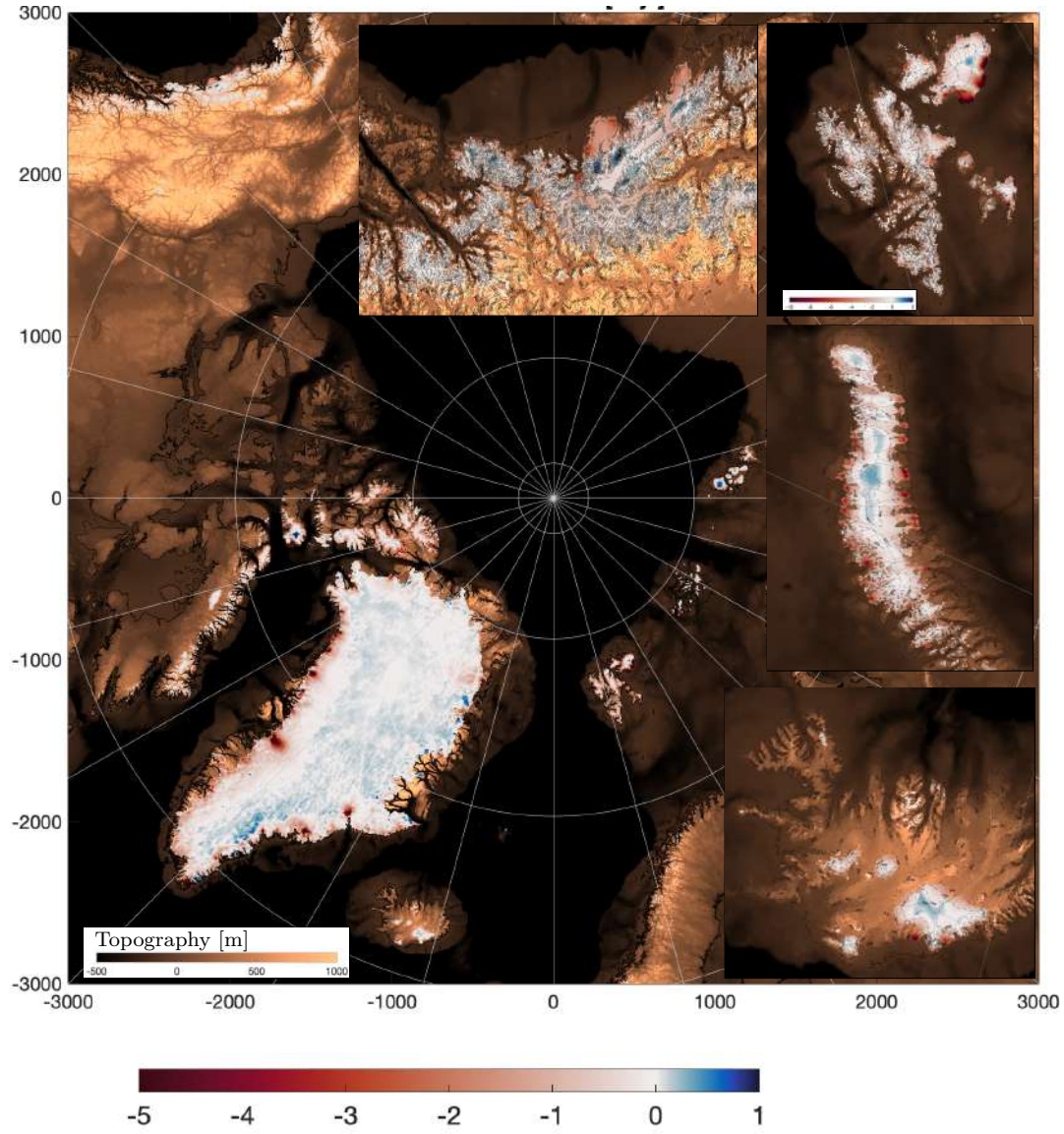

Figure S1.1. Ice elevation change from 2003 to 2015 in m yr^{-1} (red-blue scale) resulting from the redistribution explained above. The most interesting regions (Alaskian Coast, Svalbard (on a wider colorscale), Novaya Zemlja and Iceland) are enlarged. There is no significant ice loss in mainland Siberia. The elevation change is not comparable with actual elevation change, since no model for firn has been applied. The values on the map a proportional with mass changes (assumed density of 917 kg m^{-3})

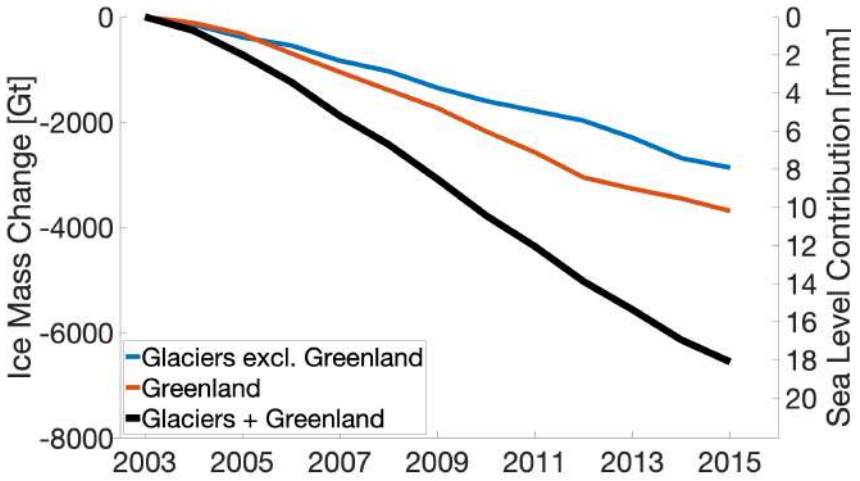

Figure S1.2. Ice loss from Greenland (including peripheral glaciers) and Arctic glaciers that goes in to the VLM calculations.

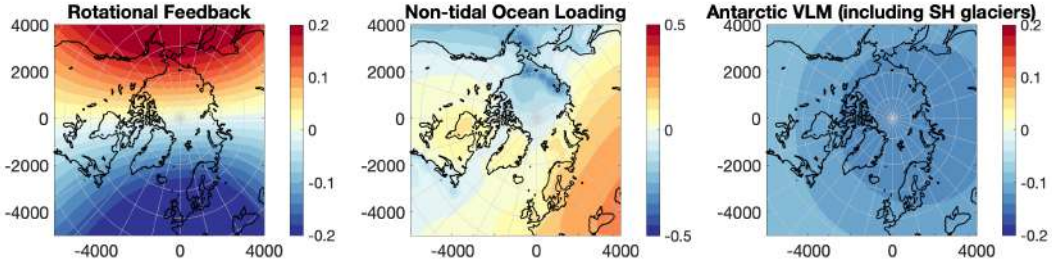

Figure S2.1. 2003-2015 average trends of rotational feedback, Non-tidal ocean loading and Antarctic elastic VLM fingerprint [mm yr^{-1}].

S2 Influence of rotational feedback, ocean loading and Antarctic ice loss

Rotational feedback is calculated using the eq.1 and eq.2 by King and Watson (2014). Pole positions x_p, y_p used in the calculations are available from `https://datacenter.iers.org/eop.php`. The Geocenter Motion subtracted from GNSS calculated as described in (Swenson et al., 2008) uses the degree-1 stokes coefficients based on the calculations by Sun et al. (2016) are available from `https://grace.jpl.nasa.gov/data/get-data/geocenter/`. The associated uncertainity of the geocenter motion has been added to the GNSS-error estimate. The elastic VLM effect of Antarctic Ice Loss is estimated from elevation changes by Schröder et al. (2019), which had an average mass loss of 105 Gt yr^{-1} between 2003 and 2015 which agrees well with the result of IMBIE(Shepherd et al., 2018).

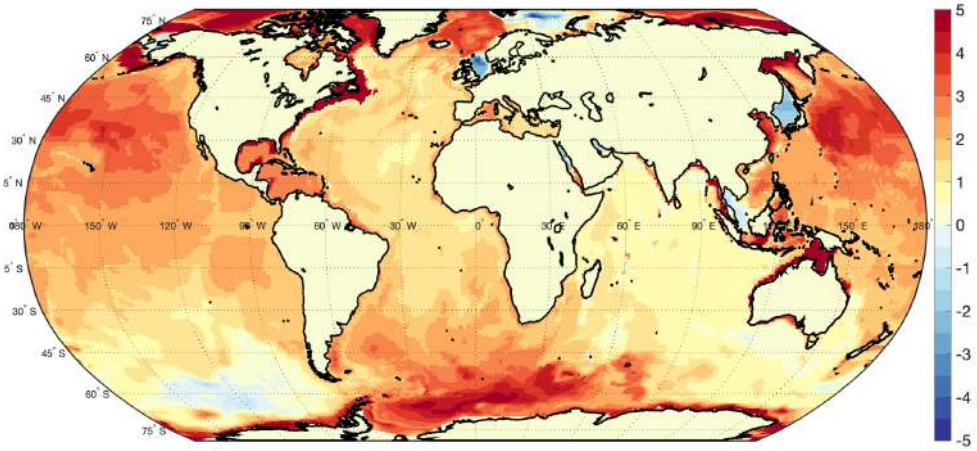

Figure S2.2. 2003-2015 ocean mass trend [mm/y] from ECCOv4r4 OBP used to estimate the effect of NOL.

S3 Spatial distributions of of the VLM-model error

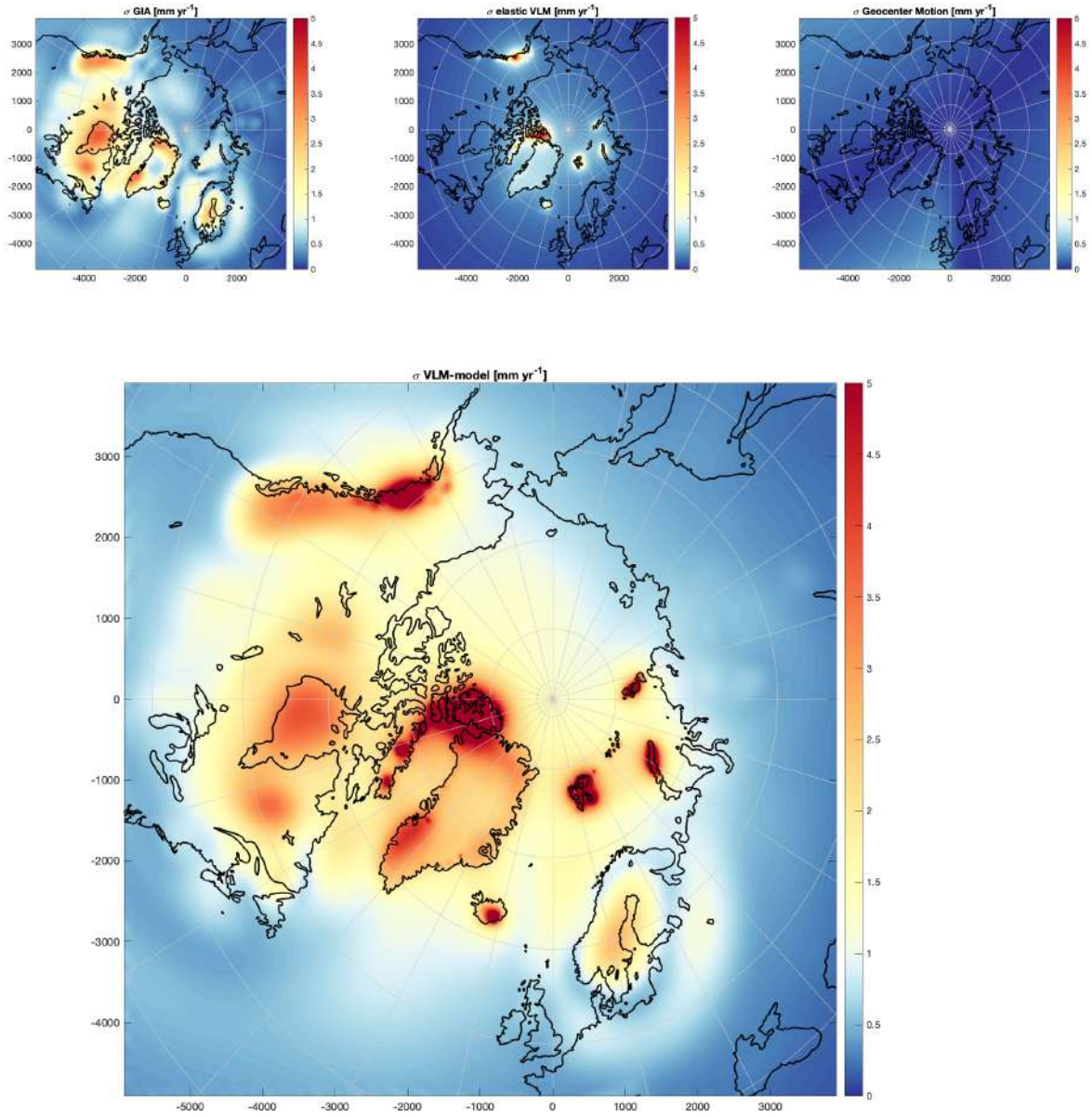

Figure S3.1. Standard deviation (σ) of GIA, elastic VLM and Geocenter Motion and combined for the total VLM-model [mm/yr] for 2003-2015.

S4 VLM at GNSS-sites

In this section, we explain the VLM measured by GNSS in comparison to the VLM-model for the regions covered in this study.

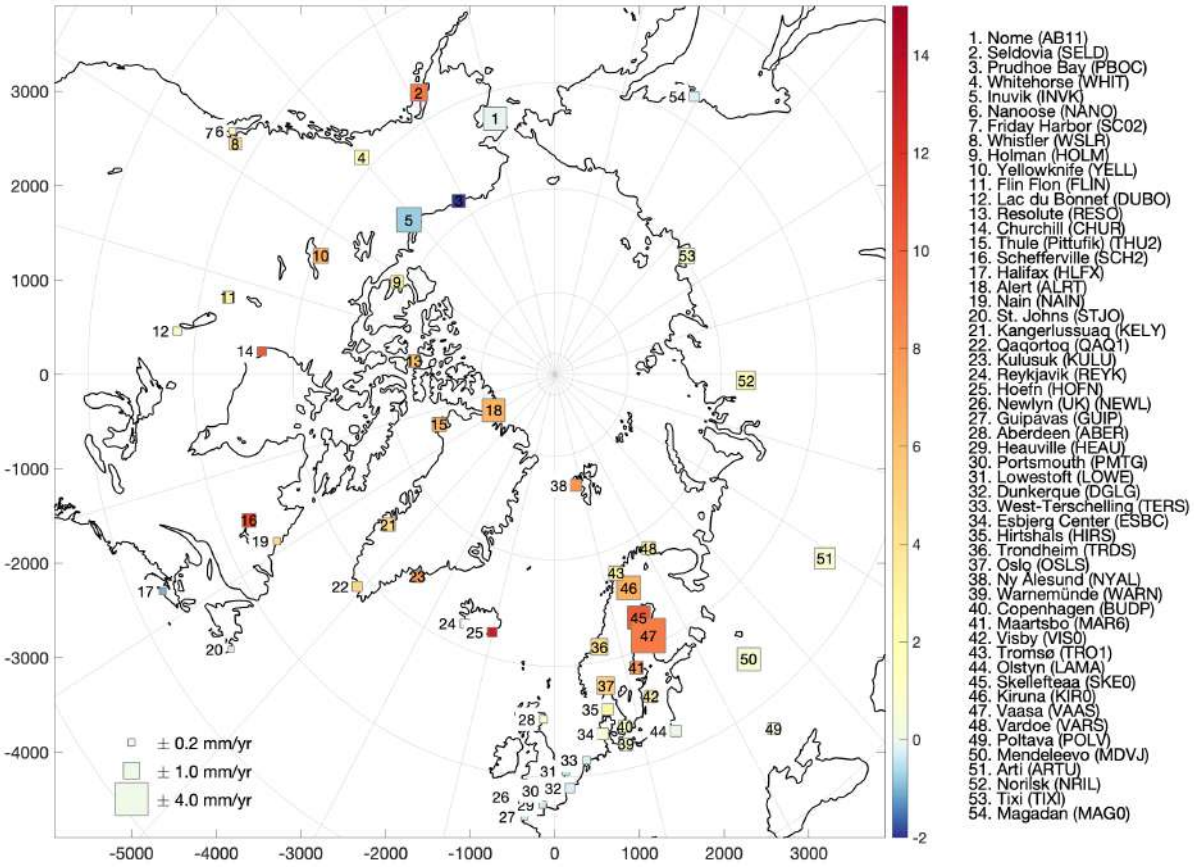

Figure S4.1. Location and name (and IGS abbreviation) of the 42 GNSS-sites used in this study ordered from most west to most east. The color indicates the linear trend from 2003-2015 [mm yr^{-1}], while the size of the square is proportional with the standard error (as estimated in the URL6-product).

S5 Timeseries of vertical deformation at all GNSS sites

Figure S5.1 shows both measured and modeled vertical deformation from 2003-2015 of each individual GNSS-site. It also reflects, how elastic VLM is changing year by year, while GIA is linear.

S6 Contribution of elastic VLM and GIA

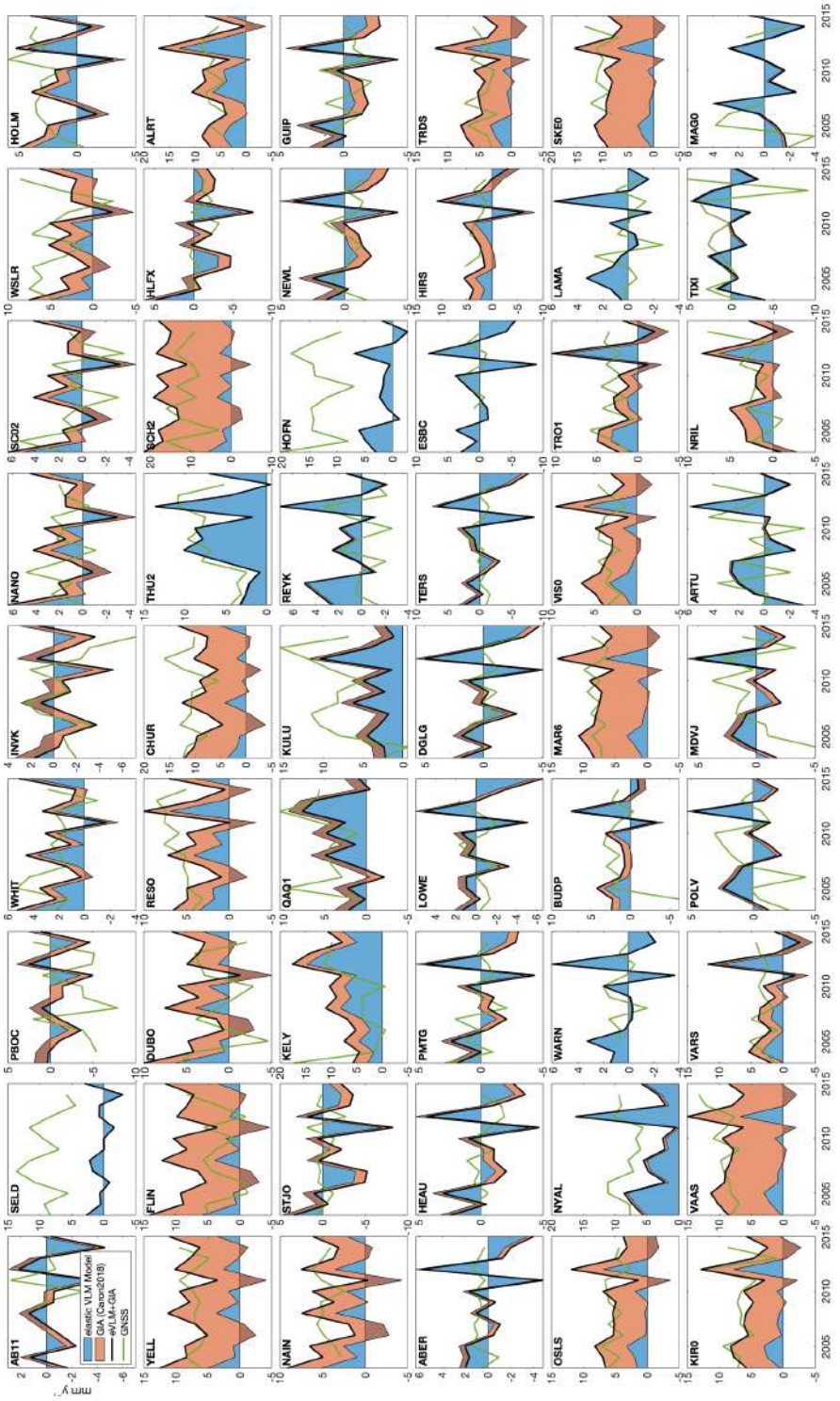

Figure S5.1. Measured and predicted year-to-year VLM-change [mm y^{-1}] from 2003 to 2015 for the 54 GNSS locations. GNSS is shown by the green line and the VLM model by the black line. The red and blue areas indicate the part of the VLM model that is elastic and GIA.

	IGS id	Abbr.	elastic VLM	Caron2018	VLM-model	GNSS VLM	Residual
Nome	4	AB11	-0.4 ± 0.7	-0.8 ± 0.3	-1.1 ± 1.0	-0.1 ± 0.9	-1.0 ± 1.4
Seldovia	517	SELD	0.3 ± 1.6	-0.1 ± 0.8	0.2 ± 2.4	9.2 ± 1.0	-9.0 ± 2.6
Prudhoe Bay	433	PBOC	0.1 ± 0.9	-1.5 ± 0.5	-1.4 ± 1.4	-3.2 ± 1.6	1.8 ± 2.1
Whitehorse	651	WHIT	1.1 ± 2.6	0.9 ± 1.3	2.0 ± 3.9	2.0 ± 0.8	0.0 ± 4.0
Inuvik	232	INVK	0.3 ± 1.0	-1.7 ± 0.9	-1.4 ± 1.9	-0.8 ± 1.0	-0.6 ± 2.1
Nanoose	341	NANO	-0.1 ± 0.6	1.5 ± 2.7	1.5 ± 3.3	1.6 ± 1.0	-0.2 ± 3.4
Friday Harbor	508	SC02	-0.2 ± 0.5	1.3 ± 2.6	1.1 ± 3.1	0.4 ± 1.3	0.7 ± 3.4
Whistler	656	WSLR	0.3 ± 0.6	2.5 ± 3.1	2.8 ± 3.8	4.5 ± 1.3	-1.7 ± 4.0
Holman	218	HOLM	0.3 ± 1.0	1.1 ± 0.8	1.4 ± 1.8	3.1 ± 1.1	-1.7 ± 2.1
Yellowknife	664	YELL	0.4 ± 0.8	7.6 ± 1.5	8.0 ± 2.3	6.8 ± 0.8	1.2 ± 2.4
Flin Flon	168	FLIN	0.2 ± 0.6	8.3 ± 1.6	8.4 ± 2.2	3.0 ± 0.9	5.4 ± 2.4
Lac du Bonnet	143	DUBO	0.1 ± 0.5	3.7 ± 1.1	3.8 ± 1.6	1.0 ± 0.9	2.8 ± 1.8
Resolute	477	RESO	1.1 ± 2.2	3.1 ± 0.9	4.2 ± 3.1	6.0 ± 1.2	-1.8 ± 3.3
Churchill	106	CHUR	0.4 ± 0.7	8.4 ± 2.8	8.8 ± 3.5	10.4 ± 0.8	-1.6 ± 3.6
Thule (Pittufik)	583	THU2	5.3 ± 3.3	0.1 ± 2.1	5.4 ± 5.4	6.6 ± 0.9	-1.2 ± 5.5
Schefferville	510	SCH2	0.4 ± 0.6	15.7 ± 2.3	16.1 ± 2.9	11.0 ± 0.7	5.0 ± 3.0
Halifax	211	HLFX	-0.5 ± 0.4	-1.5 ± 0.8	-2.0 ± 1.2	-1.1 ± 1.6	-0.9 ± 2.0
Alert	27	ALRT	3.4 ± 4.0	4.1 ± 1.5	7.6 ± 5.6	6.6 ± 1.2	1.0 ± 5.7
Nain	340	NAIN	0.4 ± 0.7	4.0 ± 1.0	4.4 ± 1.7	4.6 ± 1.5	-0.2 ± 2.3
St. Johns	548	STJO	-0.5 ± 0.4	-1.4 ± 0.3	-1.8 ± 0.8	-0.2 ± 0.8	-1.6 ± 1.1
Kangerlussuaq	247	KELY	6.6 ± 2.5	2.9 ± 3.4	9.4 ± 5.8	4.6 ± 1.2	4.8 ± 5.9
Qaqortoq	467	QAQ1	4.1 ± 1.5	-1.7 ± 1.4	2.4 ± 2.8	4.9 ± 0.8	-2.5 ± 3.0
Kulusuk	265	KULU	5.1 ± 1.6	-1.5 ± 1.0	3.6 ± 2.6	7.8 ± 1.0	-4.2 ± 2.8
Reykjavik	479	REYK	1.4 ± 1.4	0.2 ± 1.4	1.6 ± 2.8	-0.0 ± 1.1	1.6 ± 3.1
Hoefn	215	HOFN	1.9 ± 3.9	-0.1 ± 1.0	1.8 ± 4.9	13.1 ± 1.1	-11.3 ± 5.1
Newlyn (UK)	347	NEWL	0.1 ± 0.4	-1.1 ± 0.2	-0.9 ± 0.6	-0.2 ± 1.3	-0.7 ± 1.4
Guipavas	202	GUIP	0.2 ± 0.3	-1.0 ± 0.2	-0.9 ± 0.6	-0.4 ± 1.7	-0.4 ± 1.8
Aberdeen	10	ABER	0.4 ± 0.5	-0.5 ± 0.4	-0.1 ± 0.9	0.9 ± 1.2	-1.0 ± 1.5
Heauville	206	HEAU	0.1 ± 0.3	-0.8 ± 0.2	-0.7 ± 0.6	-0.3 ± 1.5	-0.4 ± 1.6
Portsmouth	446	PMTG	0.3 ± 0.4	-0.8 ± 0.3	-0.5 ± 0.6	0.1 ± 1.2	-0.6 ± 1.4
Lowestoft	286	LOWE	0.1 ± 0.4	-0.8 ± 0.5	-0.7 ± 0.9	-0.4 ± 1.8	-0.2 ± 2.0
Dunkerque	134	DGLG	0.2 ± 0.4	-0.7 ± 0.5	-0.6 ± 0.8	-0.3 ± 0.9	-0.3 ± 1.2
West-Terschelling	568	TERS	0.1 ± 0.4	-0.9 ± 0.7	-0.8 ± 1.1	-0.2 ± 0.8	-0.6 ± 1.4
Esbjerg Center	153	ESBC	0.3 ± 0.4	-0.1 ± 0.5	0.2 ± 0.9	0.6 ± 0.8	-0.4 ± 1.2
Hirtshals	210	HIRS	0.4 ± 0.5	2.2 ± 0.8	2.7 ± 1.3	2.8 ± 1.9	-0.1 ± 2.3
Trondheim	596	TRDS	0.8 ± 0.6	4.6 ± 1.1	5.4 ± 1.7	4.3 ± 0.8	1.1 ± 1.9
Oslo	378	OSLS	0.7 ± 0.5	5.0 ± 1.8	5.7 ± 2.3	5.2 ± 0.8	0.5 ± 2.4
Ny Ålesund	370	NYAL	4.6 ± 5.3	0.5 ± 0.4	5.1 ± 5.7	7.9 ± 0.9	-2.9 ± 5.7
Warnemünde	647	WARN	0.6 ± 0.4	-0.1 ± 0.5	0.5 ± 0.9	0.6 ± 0.8	-0.0 ± 1.2
Copenhagen	75	BUDP	0.6 ± 0.4	0.9 ± 0.5	1.6 ± 0.9	1.6 ± 3.7	-0.1 ± 3.8
Maartsbo	306	MAR6	0.8 ± 0.5	7.6 ± 2.4	8.3 ± 2.9	7.8 ± 0.8	0.5 ± 3.0
Visby	639	VIS0	0.8 ± 0.4	3.3 ± 1.1	4.0 ± 1.6	3.3 ± 0.8	0.8 ± 1.8
Tromsø	599	TRO1	0.9 ± 0.8	1.7 ± 0.7	2.5 ± 1.5	3.0 ± 0.8	-0.5 ± 1.7
Olstyn	274	LAMA	0.7 ± 0.4	0.1 ± 0.5	0.8 ± 0.9	-0.0 ± 0.7	0.8 ± 1.2
Skellefteaa	534	SKE0	0.9 ± 0.6	8.5 ± 2.1	9.4 ± 2.7	10.3 ± 7.0	-0.9 ± 7.5
Kiruna	252	KIR0	0.9 ± 0.7	5.2 ± 0.9	6.1 ± 1.6	6.8 ± 0.8	-0.6 ± 1.8
Vaasa	625	VAAS	0.9 ± 0.6	8.3 ± 2.2	9.1 ± 2.7	9.0 ± 0.9	0.1 ± 2.9
Vardoe	630	VARS	0.9 ± 0.8	2.0 ± 0.6	2.9 ± 1.4	3.0 ± 0.9	-0.2 ± 1.7
Poltava	452	POLV	0.7 ± 0.3	-0.4 ± 0.3	0.2 ± 0.5	0.2 ± 1.0	0.0 ± 1.1
Mendeleevo	323	MDVJ	0.8 ± 0.4	-0.7 ± 0.8	0.2 ± 1.2	0.7 ± 1.1	-0.5 ± 1.6
Arti	36	ARTU	0.8 ± 0.3	-0.2 ± 0.2	0.6 ± 0.6	0.7 ± 0.9	-0.1 ± 1.0
Norilsk	360	NRIL	0.9 ± 0.6	1.9 ± 0.2	2.8 ± 0.8	1.8 ± 0.8	1.0 ± 1.2
Tixi	587	TIXI	0.2 ± 0.6	-0.3 ± 0.3	-0.1 ± 0.9	1.0 ± 1.0	-1.1 ± 1.3
Magadan	298	MAG0	-0.2 ± 0.3	-0.2 ± 0.2	-0.4 ± 0.5	-0.3 ± 1.0	-0.1 ± 1.2

Table S4.1. Measured and modelled VLM for each GNSS-site in mm yr^{-1}. VLM-model is the sum of elastic VLM and GIA VLM.

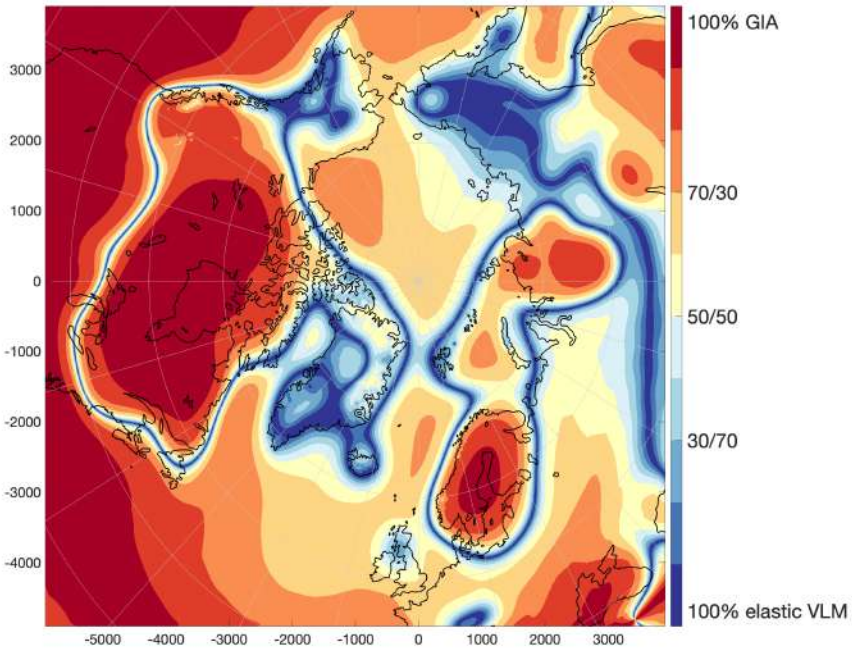

Figure S6.1. Percentage contribution of GIA-rate and elastic VLM-rate to total VLM-rate (in absolute terms) are shown. Red colors indicate areas in which GIA dominates VLM, while blue colors indicate areas in which elastic VLM is dominant.

References

King, M. A., & Watson, C. S. (2014, 09). Geodetic vertical velocities affected by recent rapid changes in polar motion. *Geophysical Journal International*, *199*(2), 1161-1165. Retrieved from https://doi.org/10.1093/gji/ggu325 doi: 10.1093/gji/ggu325

Pfeffer, W. T., Arendt, A. A., Bliss, A., Bolch, T., Cogley, J. G., Gardner, A. S., ... et al. (2014). The randolph glacier inventory: a globally complete inventory of glaciers. *Journal of Glaciology*, *60*(221), 537552. doi: 10.3189/2014JoG13J176

Schröder, L., Horwath, M., Dietrich, R., Helm, V., van den Broeke, M. R., & Ligtenberg, S. R. M. (2019). Four decades of antarctic surface elevation changes from multi-mission satellite altimetry. *The Cryosphere*, *13*(2), 427–449. Retrieved from https://www.the-cryosphere.net/13/427/2019/ doi: 10.5194/tc-13-427-2019

Shepherd, A., Ivins, E., Rignot, E., Smith, B., van den Broeke, M., Velicogna, I., ... Wouters, B. (2018). Mass balance of the antarctic ice sheet from 1992 to 2017. *Nature*, *558*(7709), 219–222. doi: 10.1038/s41586-018-0179-y

Sun, Y., Riva, R., & Ditmar, P. (2016). Optimizing estimates of annual variations and trends in geocenter motion and j2 from a combination of grace data and geophysical models. *Journal of Geophysical Research: Solid Earth*, *121*(11), 8352-8370. Retrieved from https://agupubs.onlinelibrary.wiley.com/doi/abs/10.1002/2016JB013073 doi: 10.1002/2016JB013073

Swenson, S., Chambers, D., & Wahr, J. (2008). Estimating geocenter variations from a combination of grace and ocean model output. *Journal of Geophysical Research: Solid Earth*, *113*(B8). Retrieved from https://agupubs.onlinelibrary.wiley.com/doi/abs/10.1029/2007JB005338 doi: 10.1029/2007JB005338